ATF3 protects against atherosclerosis by suppressing 25-hydroxycholesterol–induced lipid body formation

Elizabeth S. Gold,[1] Stephen A. Ramsey,[1] Mark J. Sartain,[2] Jyrki Selinummi,[3,4] Irina Podolsky,[1] David J. Rodriguez,[2] Robert L. Moritz,[2] and Alan Aderem[1]

[1]Seattle Biomedical Research Institute, Seattle, WA 98109
[2]Institute for Systems Biology, Seattle, WA 98109
[3]Department of Signal Processing, Tampere University of Technology, 33720 Tampere, Finland
[4]Quva Oy, 33720 Tampere, Finland

Atherosclerosis is a chronic inflammatory disease characterized by the accumulation of lipid–loaded macrophages in the arterial wall. We demonstrate that macrophage lipid body formation can be induced by modified lipoproteins or by inflammatory Toll–like receptor agonists. We used an unbiased approach to study the overlap in these pathways to identify regulators that control foam cell formation and atherogenesis. An analysis method integrating epigenomic and transcriptomic datasets with a transcription factor (TF) binding site prediction algorithm suggested that the TF ATF3 may regulate macrophage foam cell formation. Indeed, we found that deletion of this TF results in increased lipid body accumulation, and that ATF3 directly regulates transcription of the gene encoding cholesterol 25–hydroxylase. We further showed that production of 25–hydroxycholesterol (25–HC) promotes macrophage foam cell formation. Finally, deletion of ATF3 in *Apoe*^{−/−} mice led to in vivo increases in foam cell formation, aortic 25–HC levels, and disease progression. These results define a previously unknown role for ATF3 in controlling macrophage lipid metabolism and demonstrate that ATF3 is a key intersection point for lipid metabolic and inflammatory pathways in these cells.

CORRESPONDENCE
Alan Aderem:
alan.aderem@seattlebiomed.org

Abbreviations used: 25-HC, 25-hydroxycholesterol; acLDL, acetylated low-density lipoprotein; BMDM, BM-derived macrophage; CE, cholesteryl ester; oxLDL, oxidized LDL; TF, transcription factor; TG, triglyceride; TLR, toll-like receptor.

Cardiovascular disease is the leading cause of mortality and morbidity globally (World Health Organization Fact Sheet no. 317, http://www.who.int/mediacentre/factsheets/fs317/en/index.html). Atherosclerosis, a key underlying mechanism in cardiovascular disease, is a chronic inflammatory condition, characterized by focal thickening of artery walls and the formation of lipid-rich atheromatous lesions (i.e., plaques). These lesions contain abundant lipid-laden macrophage foam cells (Lundberg, 1985). The interaction between lipid metabolism and inflammation in plaque macrophages has been implicated in atherosclerosis progression (Moore and Tabas, 2011, and references therein) but much remains unknown about how the interaction of these two processes is controlled at the transcriptional level.

Many features of lipid bodies suggest that they represent an intersection point between macrophage inflammatory and metabolic pathways.

Cytoplasmic lipid bodies contain a core of triglycerides (TGs) and cholesteryl esters (CEs) surrounded by a monolayer of phospholipids and proteins (Melo et al., 2011). In atherosclerotic plaque, uncontrolled uptake of oxidized low-density lipoprotein (oxLDL) by macrophages through scavenger receptors causes TG and cholesterol loading, followed by cholesterol esterification and storage of CE in cytoplasmic lipid bodies (Maxfield and Tabas, 2005; Greaves and Gordon, 2005). Lipid body formation in macrophages is also induced by a variety of inflammatory stimuli, such as Toll-like receptor (TLR) agonists (Nicolaou and Erridge, 2010). Although lipid bodies have previously been thought to simply provide neutral lipid storage, it has recently become clear that they are highly regulated and functionally active organelles (Imanishi et al., 2004;

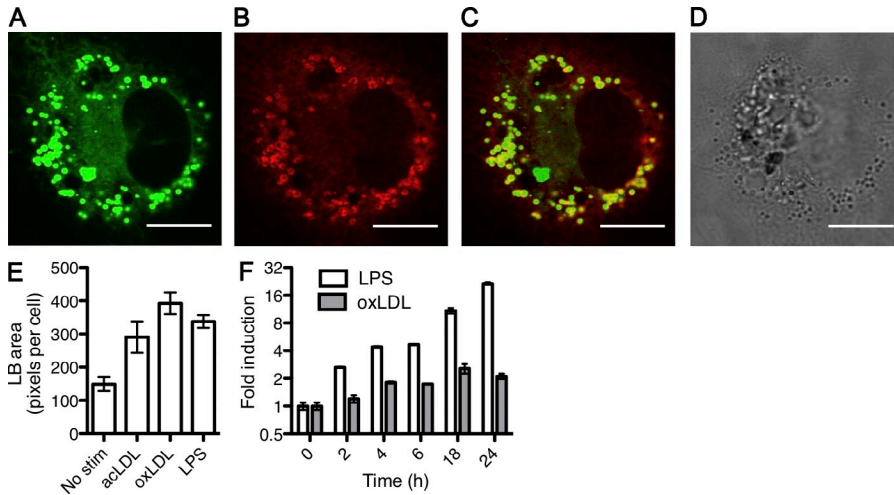E.S. Gold and S.A. Ramsey contributed equally to this paper.

Figure 1. Endotoxin- and lipoprotein-induced neutral lipid accumulations colocalize with lipid body marker ADRP. (A–C) WT BMDMs were stimulated with 5 µg/ml acetylated LDL (acLDL) for 4 h, stained for neutral lipids (BODIPY 493/503) and immuno-fluorescence–stained for the lipid body marker protein ADRP (adipose differentiation related protein, also known as PLIN2). ADRP detection was using an Alexa Fluor 633–conjugated secondary antibody. (For a BODIPY image of unstimulated macrophages, see Fig. 2 C). (A) BODIPY fluorescence shown in green. (B) Alexa Fluor 633 (ADRP) fluorescence shown in red. (C) Overlay. (D) Phase-contrast bright-field image showing refractile droplets that colocalize with BODIPY- and ADRP-positive lipid bodies. Images shown are from a representative of two independent experiments. Bars, 10 µm. (E) Quantitation of mean area per cell, occupied by BODIPY-positive lipid bodies in stacked confocal epifluorescence micrographs of WT BMDM stimulated for 18 h with 5 µg/ml acLDL, 5 µg/ml oxLDL, or 100 ng/ml LPS. Error bars represent the mean ± SEM (five fields per condition) from a representative experiment (two independent experiments performed). (F) Time course of mRNA levels of *Atf3* in WT BMDM treated with 25 µg/ml oxLDL or 10 ng/ml LPS, as measured by qPCR (normalized to *Eef1a1*). Error bars represent the mean ± SEM (two independent biological replicates).

Bozza et al., 2007; Silva et al., 2009). The observation that key enzymes involved in cholesterol metabolism and fatty acid synthesis localize to lipid bodies suggests that they are also sites for lipid metabolic activity (Fujimoto et al., 2004; Zhao et al., 2005). Additionally, lipid bodies have been shown to contain eicosanoid-forming enzymes and have been demonstrated to be sites for eicosanoid generation (Silva et al., 2009).

ATF3 (activating transcription factor 3), a member of the CREB family of basic leucine zipper transcription factors (TFs), has been shown to be involved in both inflammatory and metabolic pathways (Gilchrist et al., 2006; Zmuda et al., 2010). ATF3 is transcriptionally induced in response to various conditions that are associated with macrophage foam cell formation in atherosclerotic plaques including oxidative stress, hypoxia, cytokines, and ER stress (Hai et al., 1999; Okamoto et al., 2006; Chen et al., 2008; Seimon et al., 2010). Notably, ATF3 is expressed at higher levels in human atherosclerotic vessels than in nonatherosclerotic vessels, and ATF3 is strongly expressed in macrophages within atherosclerotic vessels (Nawa et al., 2002). Activation of macrophage TLRs has been shown to play a role in the progression of atherosclerosis, and we have previously demonstrated that ATF3 is up-regulated early after TLR engagement and that it acts as a negative regulator of TLR induced cytokine production in macrophages (Gilchrist et al., 2006).

25-hydroxycholesterol (25-HC) is a metabolite of cholesterol that is produced and secreted by macrophages and has multiple effects on immune responses and cholesterol metabolism in these cells. This oxysterol has been shown to suppress the production of IgA by B cells (Bauman et al., 2009), alter B cell migration (Pereira et al., 2010), and control the differentiation of monocytes into macrophages (Ecker et al., 2010). 25-HC has long been known to suppress cholesterol biosynthesis (Kandutsch and Chen, 1975; Miller and Melnykovych, 1984) and inhibit expression of genes involved in fatty acid and cholesterol synthesis (Trzaskos et al., 1989; Field et al., 2001). 25-HC has also been shown to stimulate CE formation (Brown et al., 1975; Miller and Melnykovych, 1984). The enzyme Ch25h (cholesterol 25-hydroxylase), which catalyzes the formation of this oxysterol, has been demonstrated to be transcriptionally up-regulated after activation of macrophages by TLR agonists (Bauman et al., 2009; Diczfalusy et al., 2009; Park and Scott, 2010). However, the transcriptional regulatory events that induce production of this enzyme after TLR activation are not fully understood.

In the present study, we used an unbiased systems biology approach to determine that ATF3 is a key transcriptional regulator of the process of lipid body formation in macrophages. We provide evidence that the effect of ATF3 on lipid body formation is mediated through direct binding to the promoter of the gene *Ch25h*, which leads to epigenetic repression of *Ch25h* transcription. We demonstrate that loss of ATF3 leads to increased macrophage foam cell formation

Table 1. National Center for Biotechnology Information GEO accession numbers for microarray datasets

Strains	Conditions	Affymetrix GeneChip type	GEO accession no.
WT and *Atf3*⁻/⁻	Unstimulated, oxLDL (24 h)	Mouse Exon 1.0 ST Array	GSE32358
WT	Unstimulated, LPS (4 h)	Mouse Exon 1.0 ST Array	GSE32359
WT and *Atf3*⁻/⁻	Unstimulated, LPS (4 h)	Mouse Genome 430 2.0 Array (3′ array)	GSE32574

in vivo. Finally, we show that the severity of aortic root athero-sclerosis in a mouse model of diet-induced disease (the $Apoe^{-/-}$ mouse; Smith and Breslow, 1997) is accelerated by loss of ATF3 and that this correlates with increased levels of 25-HC in aortas from $Atf3^{-/-}$ animals relative to matched controls. Our data demonstrate a previously unknown role for ATF3 in controlling lipid metabolism in the macrophage and show that this TF is a key intersection point for lipid metabolic and inflammatory pathways in these cells.

RESULTS

Identification of ATF3 as a transcriptional regulator of lipid body formation in macrophages

BM-derived macrophages (BMDMs) stimulated with either modified lipoproteins or the TLR agonist LPS accumulate large numbers of lipid bodies, as determined by confocal microscopy (Fig. 1, A–D) and by quantitative image analysis (Fig. 1 E). To identify potential transcriptional regulators of lipid body formation, we undertook a global unbiased screen for TFs that are activated by both modified lipoproteins and LPS. Our strategy was as follows. First, we used microarray transcriptome profiling data from WT C57BL/6J BMDM to identify two groups of transcripts that are up-regulated by LPS treatment (Table S1, top 259 rows) and by oxLDL treatment (Table S2, top 35 rows), respectively. To narrow our search for cis-regulatory elements within the promoter regions corresponding to these transcripts, we took advantage of the observation that histone acetylation is associated with sites of TF binding to chromatin (Vettese-Dadey et al., 1996; Ramsey et al., 2010b) and that using histone acetylation data to guide a genomic sequence-based computational search for TF binding sites improves the accuracy of binding site prediction by ∼40% (Ramsey et al., 2010b). Specifically, we performed a genome-wide chromatin immunoprecipitation assay with sequence-based detection (ChIP-seq), with an antibody to acetylated histones, in BMDM stimulated with either LPS or oxLDL (Table S3). Next, we tabulated all histone-acetylated regions within the promoters of the LPS- or oxLDL-responsive transcripts, and computationally scanned the regions for TF binding site sequence elements. This analysis identified eight sequence elements that were statistically over-represented within both the LPS- and oxLDL-associated promoter regions and that corresponded to TFs that were detected above background on the microarray (ATF3, TGIF1, AP1, LXR, GATA1, ZFP281, REST, and TAL1). Only the gene $Atf3$ had strong differential expression under both LPS stimulation and oxLDL stimulation (data provided as indicated in Table 1). Quantitative PCR (qPCR) analysis of BMDM stimulated with oxLDL or LPS confirmed that $Atf3$ is up-regulated by these stimuli (Fig. 1 F). Collectively, these results suggested that ATF3 represents an intersection point for metabolic and inflammatory responses in macrophages by controlling lipid body formation.

To test this hypothesis, we compared the neutral lipid content of $Atf3^{-/-}$ and WT BMDM using flow cytometry for the neutral lipid fluorophore BODIPY. The difference in
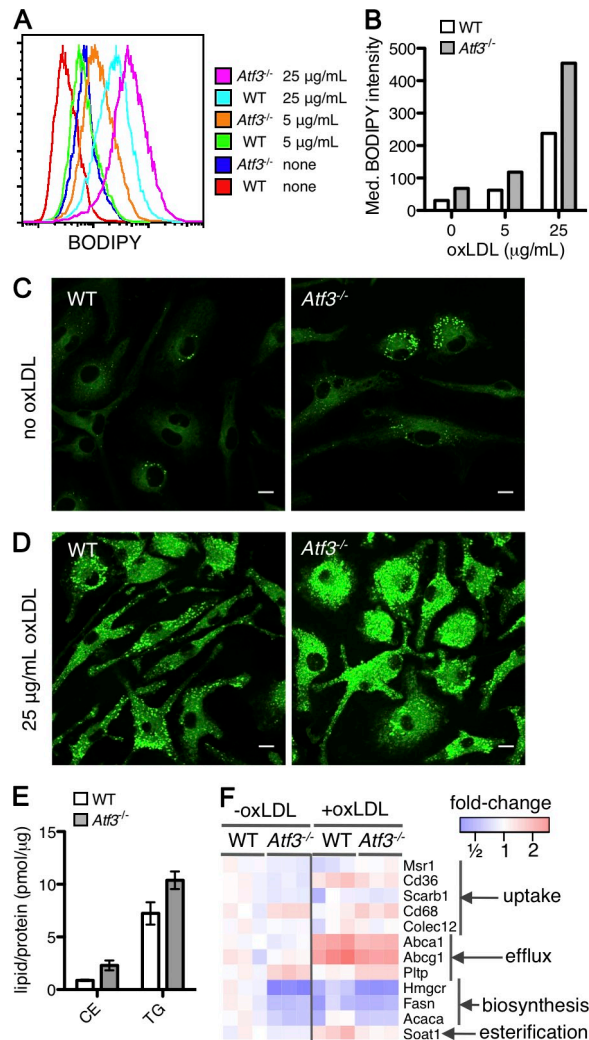

Figure 2. $Atf3^{-/-}$ macrophages have higher neutral lipid content than WT macrophages in the presence (or absence) of oxLDL. (A) Flow cytometry fluorescence histograms of BODIPY-stained BMDM of the indicated genotypes, incubated for 24 h with oxLDL at the indicated concentrations. (B) $Atf3^{-/-}$ and WT BMDM were incubated for 24 h in medium containing 0, 5, or 25 µg/ml oxLDL. BODIPY-stained median fluorescence levels are shown. (C and D) Confocal epifluorescence micrographs of BODIPY-stained BMDM of the indicated genotypes incubated without (C) or with (D) 25 µg/ml oxLDL for 24 h. Bars, 10 µm. Images shown are from a representative of two independent experiments. (E) Quantitative assay for cellular CE and TG, normalized to total protein content, in BMDM of the indicated genotypes. Error bars represent mean ± SEM (three independent biological replicates). (F) Heat map showing relative transcript levels for 10 genes based on oligonucleotide microarray hybridization (exon array). Each column represents a single biological replicate for BMDM of the indicated genotype and condition (no oxLDL or 25 µg/ml oxLDL for 24 h), and each row represents a gene. Color indicates expression level relative to the gene's mean expression level in WT unstimulated BMDM. As shown in the heat map, microarray profiling of each genotype and condition was performed in three biological replicates.

cell population median BODIPY fluorescence intensity (ΔI) between $Atf3^{-/-}$ and WT BMDM was larger for cells incubated with 25 µg/ml oxLDL ($\Delta I = 216$) or with 5 µg/ml oxLDL
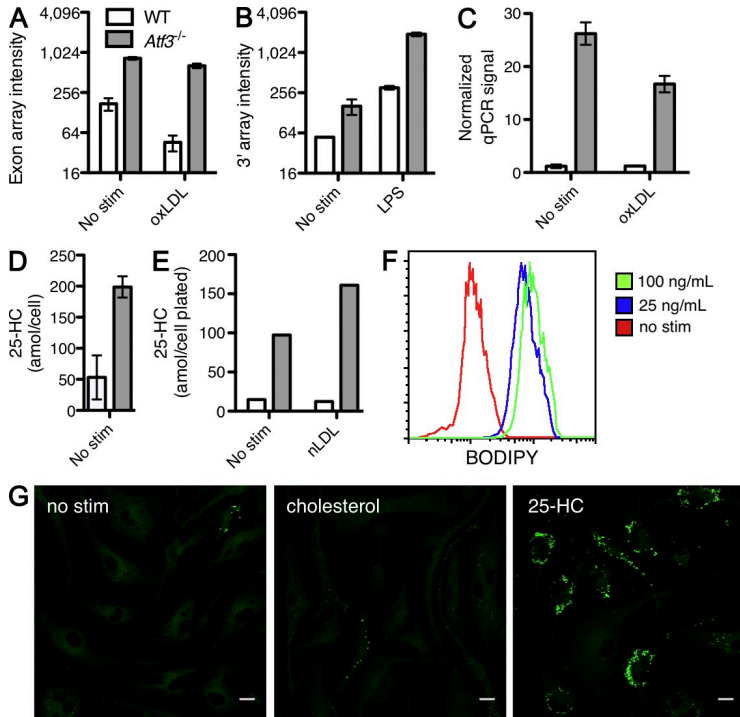
Figure 3. *Ch25h* transcript level and 25-HC are up-regulated in *Atf3*−/− versus WT macrophages. (A) *Ch25h* transcript levels in BMDM incubated with media alone or with 25 µg/ml oxLDL for 24 h, measured by exon microarray. Error bars represent the mean ± SEM (n = 3). (B) *Ch25h* transcript levels in BMDM incubated with media alone or with 10 ng/ml LPS for 4 h, measured by 3′ gene expression microarray. Error bars represent the mean ± SEM (n = 3 experiments for each bar, except for LPS *Atf3*−/−, for which n = 2). (C) Relative transcript levels of *Ch25h* in BMDM of the indicated genotypes incubated with no oxLDL or with 25 µg/ml oxLDL for 24 h, as measured by qPCR (normalized to *Gapdh*). Error bars represent the mean ± SEM (n = 3). (D) Levels of free 25-HC in cell extracts from BMDM of the indicated genotypes, measured by mass spectrometry with absolute quantitation. Error bars represent the mean ± SEM (n = 2). (E) Levels of free 25-HC in medium conditioned with BMDM of the indicated genotypes and conditions (nLDL = native LDL, 25 µg/ml) for 24 h, measured by mass spectrometry. (F) BODIPY fluorescence histograms of BMDM treated with the indicated concentrations of 25-HC for 4 h. Data shown are from a representative of two independent experiments. (G) BODIPY fluorescence micrographs of WT BMDM grown for 24 h in medium alone, 25 ng/ml cholesterol, or 25 ng/ml 25-HC. Bars, 10 µm. Images shown are from a representative of three independent experiments.

(ΔI = 55) than for untreated BMDM (ΔI = 38; Fig. 2, A and B). By confocal microscopy of BODIPY-stained BMDM, the increased fluorescence of *Atf3*−/− versus WT BMDM is seen to be the result of an increased amount of cytosolic lipid bodies (Fig. 2, C and D). To determine the nature of the neutral lipids that were increased, unstimulated BMDMs were assayed by lipidomic profiling using mass spectrometry. Overall, *Atf3*−/− BMDM had 2.6-fold more CE and 1.4-fold more TG than WT BMDM (Fig. 2 E).

To gain insight into the mechanism by which ATF3 controls macrophage lipid body formation, we performed transcriptome profiling of *Atf3*−/− and WT BMDM treated with oxLDL and compared them to untreated control cells. Based on the transcriptional data, the increased CE content of *Atf3*−/− versus WT macrophages could not be attributed to increased expression of transcripts encoding lipoprotein-recognizing scavenger receptors (*Msr1*, *Cd36*, *Scarb1*, *Cd68*, and *Colec12*; list obtained from Greaves and Gordon, 2009), the rate-limiting enzyme in the cholesterol biosynthesis pathway (*Hmgcr*), fatty acid synthesis enzymes (*Acaca* and *Fasn*), or sterol *O*-acyltransferase 1 (*Soat1*) in *Atf3*−/− versus WT BMDM (Fig. 2 F). Furthermore, the increased CE content could not be attributed to decreased expression of cholesterol efflux-related transcripts (Fig. 2 F, *Abca1*, *Abcg1*, and *Pltp*) in *Atf3*−/− versus WT BMDM.

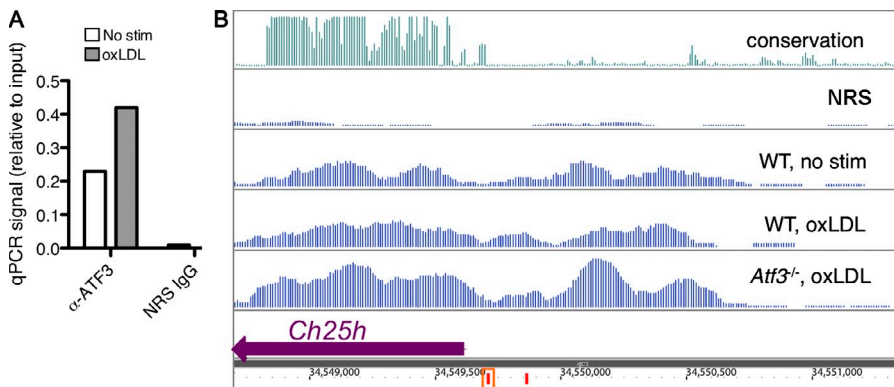**Figure 4. ATF3 binds the promoter of *Ch25h* and histone acetylation at the *Ch25h* promoter is significantly increased in *Atf3*−/− versus WT macrophages.** (A) ChIP-qPCR signal, relative to input chromatin, for WT BMDM under the indicated stimulus conditions and using the indicated antibodies (α-ATF3 or IgG from normal rabbit serum, NRS). (B) View of the *Ch25h* promoter region on mouse chromosome 19, showing histone acetylation ChIP-seq data, CREB/ATF binding elements, and conservation data. ChIP-seq data tracks (vertical blue bars at 10 bp intervals) are from BMDM of the indicated genotypes and conditions (oxLDL, 25 µg/ml for 24 h) immunoprecipitated with an antibody for acetyl-H4 or with NRS IgG as a negative control. All ChIP-seq tracks are in tags per million and are on the same vertical scale. The conservation data track (vertical green bars at 10 bp intervals, top row) are PHAST 30-way vertebrate conservation scores from genomic sequence, averaged over the flanking 10 bp. Red vertical bars denote sequence matches to the CREB/ATF TF binding site motif. The orange square indicates the locus that was assayed for ATF3 binding, by ChIP-qPCR. The *Ch25h* gene is shown at the bottom of the diagram (thick purple bar); the direction of transcription is to the left.

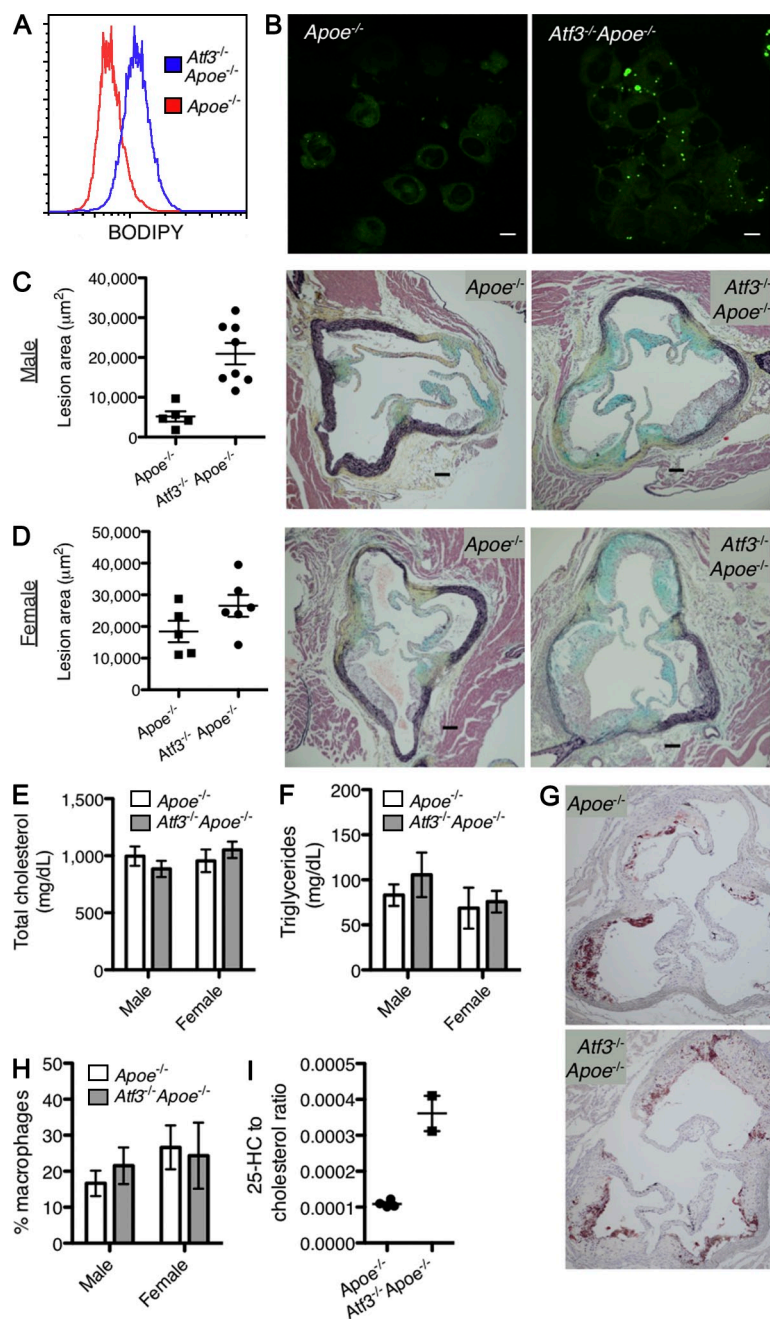ATF3 suppresses lipid body formation and atherosclerosis | Gold et al.

Figure 5. Loss of ATF3 increases neutral lipid content and lipid body formation in macrophages from hypercholesterolemic mice, increases severity of atherosclerosis and increases the level of 25–HC in aortic tissue. Mice of the indicated genotypes were maintained on a high-fat diet for 8 wk. (A) Flow cytometry fluorescence histograms for BODIPY-stained resident peritoneal macrophages (B) Confocal epifluorescence micrographs of Nile red–stained resident peritoneal macrophages. Bars, 10 µm. (C and D) Left panels show aortic root lesion areas in male (C) and female (D) mice. Long horizontal bar denotes mean, and the error bars denote SEM (each data mark denotes an individual animal). Middle and right panels show representative micrographs of aortic root sections, after Movat's pentachrome staining. Bars, 100 µm. (E) Total cholesterol and (F) TG measurements from serum. Error bars denote mean $\pm$ SEM ($n = 6$ for males, $n = 4$ for $Apoe^{-/-}$ female, and $n = 5$ for $Atf3^{-/-}Apoe^{-/-}$ female). (G) Oil red O– and hematoxylin-stained aortic root micrographs. Images shown are representative of two independent biological replicates. Bars, 100 µm. (H) Percentage of lesion section area staining positive for the macrophage marker Mac-2, by immunohistochemistry. Error bars represent the mean $\pm$ SEM (numbers of animals same as for cholesterol). (I) Ratio of 25-HC to cholesterol level, measured by mass spectrometry with absolute quantitation, in sterols isolated from homogenized aortas ($P < 0.01$, 3.3-fold increase between $Apoe^{-/-}$ and $Atf3^{-/-}Apoe^{-/-}$). The long horizontal bar denotes the mean, and the short bars denote the SEM (each data mark denotes an individual aorta; $n = 2$ for $Atf3^{-/-}Apoe^{-/-}$, one female and one male; $n = 4$ for $Apoe^{-/-}$, two females and two males). Data shown are representative of two independent experiments.

by mass spectrometry in both BMDM cell extracts (Fig. 3 D) and in BMDM-conditioned medium (Fig. 3 E). These observations, together with previous data that 25-HC promotes cholesterol esterification in macrophages, led us to hypothesize that increased 25-HC levels in $Atf3^{-/-}$ macrophages would promote foam cell formation. We therefore stimulated WT BMDM with 25 ng/ml 25-HC (which corresponds to a per-cell amount that is approximately equivalent to the amount by which 25-HC levels increase in $Atf3^{-/-}$ vs. WT macrophages) and observed, using both flow cytometry (Fig. 3 F) and confocal microscopy (Fig. 3 G), that 25-HC induces lipid body formation.

To investigate whether ATF3 directly controls the level of *Ch25h* transcriptional activity in macrophages, we performed ChIP using an antibody directed against ATF3. We found that ATF3 binds a predicted CREB/ATF binding site in the *Ch25h* promoter (Fig. 4, A and B). We have previously demonstrated that ATF3 binds histone deacetylase 1 (HDAC1) in TLR-activated macrophages and that it acts as a negative regulator by epigenetic modification of cytokine gene promoters (Gilchrist et al., 2006). We therefore examined the histone acetylation within the *Ch25h* promoter using ChIP-seq and

ATF3 controls lipid body formation by epigenetic repression of *Ch25h*

In the microarray study, the most strongly up-regulated gene in unstimulated $Atf3^{-/-}$ versus WT BMDM (two-way ANOVA test; Table S4) was *Ch25h*, encoding cholesterol 25-hydroxylase (Fig. 3 A). Intriguingly, this gene is also strongly induced by LPS (Fig. 3 B). qPCR confirmed that loss of ATF3 leads to large increases in the level of *Ch25h* mRNA in unstimulated macrophages (25-fold) and in oxLDL-stimulated macrophages (14-fold; Fig. 3 C). The increased levels of *Ch25h* mRNA in $Atf3^{-/-}$ BMDM correlated with increased levels of the enzyme's product, 25-HC, as determined

found that, as with cytokines, the loss of ATF3 in macrophages increased the level of expression of this gene through increased histone acetylation at this locus (Fig. 4 B).

Loss of ATF3 promotes atherosclerosis in ApoE knockout mice

These findings led us to speculate that targeted disruption of ATF3 may lead to increased macrophage foam cell formation and increased atherosclerosis in mice. To test this hypothesis, $Atf3^{-/-}$ mice were bred with the atherosclerosis-prone $Apoe^{-/-}$ (apolipoprotein E deficient) mouse strain, and the mice were maintained on high-fat diet for 8 wk, a time point at which aortic root lesions in this model would be expected to be macrophage-rich (Nakashima et al., 1994). Consistent with the in vitro findings described in the previous section, we observed greater neutral lipid content (Fig. 5 A) and increased lipid body formation (Fig. 5 B) in resident peritoneal macrophages isolated from the $Atf3^{-/-} Apoe^{-/-}$ animals versus from $Apoe^{-/-}$ animals.

Analysis of the extent of atherosclerotic plaque in the aortic root of the $Atf3^{-/-} Apoe^{-/-}$ and $Apoe^{-/-}$ animals demonstrated that loss of ATF3 leads to increased severity of atherosclerosis after 8 wk on high-fat diet ($P < 0.001$; Fig. 5, C and D). There was no significant difference in overall serum cholesterol (Fig. 5 E) or in the serum TG levels (Fig. 5 F) between the genotypes. Aortic root micrographs revealed that neutral lipid accumulation is predominantly cellular in both genotypes (Fig. 5 G). There was no significant difference in the macrophage (Fig. 5 H), smooth muscle cell, or T cell (not depicted) content of aortic root sections between the genotypes. Furthermore, there were no significant differences between the genotypes, in the serum levels of the inflammatory cytokines TNF, IL-1β, IL-6, MCP-1, MIP1α, or MIP1β as detected by ELISA (unpublished data).

Based on our in vitro studies, we conjectured that enhanced local production of 25-HC by plaque macrophages might contribute to the atherosclerosis phenotype in $Atf3^{-/-} Apoe^{-/-}$ versus $Apoe^{-/-}$ animals. Because 25-HC is thought to be primarily produced enzymatically in rodents (Johnson et al., 1994), we hypothesized that elevated expression of Ch25h in plaque macrophages would lead to an increased ratio of 25-HC to cholesterol in the aortas of atherosclerotic mice. To test this hypothesis, lipid extracts from aortas were analyzed by quantitative mass spectrometry for 25-HC and for cholesterol. This analysis demonstrated an increase in the 25-HC/cholesterol ratio in the aortas of $Atf3^{-/-} Apoe^{-/-}$ versus $Apoe^{-/-}$ animals (Fig. 5 I).

DISCUSSION

Atherosclerosis is a complex disease involving the dysregulation and interaction of inflammatory and metabolic pathways. The accumulation of lipid bodies in macrophages in the arterial intima, resulting in foam cell formation, is thought to be a key driver of atherogenesis. Although much is known about the mechanisms of foam cell formation, we lack complete knowledge of the TFs and lipid mediators that modulate this process and how dysregulation of the dynamic interactions between them leads to disease. The inflammatory and metabolic

pathways in macrophages are regulated at a variety of levels that include cross talk and feedback between signaling pathways (Castrillo and Tontonoz, 2004). Systems biology provides a framework in which this complexity can be addressed (Zak and Aderem, 2009; Ramsey et al., 2010a). Systems approaches combine prior biological knowledge with global measurement technologies and computational methods to both reveal regulatory interactions and place them in a network context (Gilchrist et al., 2006; Ramsey et al., 2008; Litvak et al., 2009; Zak et al., 2011). The present work has used a novel systems approach to uncover candidate transcriptional regulators of the inflammatory and metabolic pathways leading to macrophage foam cell formation. We used transcriptome profiling to identify transcripts that are up-regulated by lipid body-inducing stimuli, and then identified histone-acetylated regions within the promoters of these transcripts that may indicate chromatin accessibility to regulatory factors. These regions were computationally scanned to identify a list of candidate TFs, which was further filtered using transcriptome measurements.

This approach implicated the regulator ATF3, which we have previously demonstrated to be a negative regulator of the macrophage transcriptional response to inflammatory stimuli (Gilchrist et al., 2006). The work presented here demonstrates that ATF3 also regulates lipid metabolic pathways in the macrophage, at both basal and high levels of cellular lipid loading, and that it appears to function through a regulatory circuit involving epigenetic repression at the promoter of the cholesterol 25-hydroxylase gene *Ch25h*. Under loss of ATF3, the transcript level of Ch25h is highly up-regulated in macrophages, in both the unstimulated state and in the presence of LPS or oxLDL. We note that *Ch25h* has also been reported to be transcriptionally up-regulated in $Atf3^{-/-}$ versus WT mouse embryonic fibroblasts (Kim et al., 2010). Our findings establish that, in the absence of ATF3, the normal feedback mechanism that controls the Ch25h enzyme and its product 25-HC is lost, leading to high levels of macrophage production of 25-HC and the accumulation of 25-HC in the aorta. On the phenotypic level, in the $Apoe^{-/-}$ mouse model of diet-induced atherosclerosis, loss of ATF3 was found to accelerate aortic root atherosclerosis. As shown in Figs. 2 F and 5, we were unable to detect differences in serum lipid levels, serum cytokine levels, macrophage scavenger receptor transcript expression, cholesterol efflux-related transcript expression, or plaque cellular composition (macrophages, T cells, or SMCs) that could account for this phenotype. Notably, although female mice had larger basal lesion area (consistent with previous observations; Caligiuri et al., 1999), loss of ATF3 led to a greater increase in lesion area in male mice than in female mice, an interesting area for possible future investigation.

Our findings on the role of 25-HC are both consistent with and extend prior studies. 25-HC suppresses cholesterol synthesis largely through inhibition of 3-hydroxy-3-methylglutaryl-CoA-reductatase (Kandutsch and Chen, 1975), both through transcriptional repression of the *Hmgcr* gene and accelerated degradation of the enzyme (Trzaskos et al., 1989; Taylor, 1992). Correspondingly, our array data demonstrate that the transcript

level for *Hmgcr* is suppressed in cells from *Atf3*$^{-/-}$ mice (Fig. 2 F). Treatment of macrophages or fibroblasts with 25-HC has also been reported to increase the amount of cellular CE (Brown et al., 1975; Miller and Melnykovych, 1984), and this increase has been attributed to increased availability of cholesterol to ACAT, and not to increased ACAT activity (Miller and Melnykovych, 1984; Du et al., 2004). Correspondingly, we observed that lipid body formation and neutral lipids are increased in response to excess levels of 25-HC in *Atf3*$^{-/-}$ macrophages, and that cellular CEs in particular are significantly increased in *Atf3*$^{-/-}$ versus WT macrophages (Fig. 2 E). 25-HC is known to be a ligand for the oxysterol-activated TF LXR (Shibata and Glass, 2010) and, in that context, would be assumed to activate transcription of genes involved in reverse cholesterol transport. Our results suggest that this is not its dominant role, as we do not observe increased transcript levels of known LXR targets, such as *Abca1* or *Abcg1*, in *Atf3*$^{-/-}$ versus WT macrophages (Fig. 2 F). Intriguingly, it has been reported that genetic knockout of the 25- and 27-HC–metabolizing hepatic enzyme *Cyp7b1* (which leads to high serum levels of 25-HC [Bauman et al., 2009] and 27-HC [Li-Hawkins et al., 2000]), in the context of the *Apoe*$^{-/-}$ mouse atherosclerosis model, leads to increased aortic root lesion area (Umetani M., D.J. Mangelsdorf, and P.W. Shaul. 2010. Mechanisms of atherosclerosis: new lessons from mouse models. Abstr. 18427.).

Our data implicate ATF3 as a transcriptional regulator that controls foam cell formation; however, given the complexity of the process it is likely that other factors are involved in regulating foam cell formation. Furthermore, it is possible that loss of ATF3 contributes to lesion progression through additional pathways, such as through increased apoptosis of vascular endothelial cells (Nawa et al., 2002). One of the strengths of the systems biology approach is that it allows the integration of multiple interacting networks. The current work lays the foundation for the expansion of the ATF3 network that, in turn, will enable a more comprehensive understanding of the regulatory circuits that control the macrophage differentiation during foam cell formation leading to the progression of atherosclerosis.

MATERIALS AND METHODS
Mice
C57BL/6J (WT) and *Apoe*$^{-/-}$ (B6.129P2-*Apoe*^{tm1Unc}/J) mice were obtained from the Jackson Laboratory. *Atf3*$^{-/-}$ mice congenic to the C57BL/6 background (backcrossed > 10 generations) were a gift from T. Hai (Ohio State University, Columbus, OH; Hartman et al., 2004). *Atf3*$^{-/-}$*Apoe*$^{-/-}$ mice were generated by breeding *Atf3*$^{-/-}$ and *Apoe*$^{-/-}$ mice. For experiments involving WT and *Atf3*$^{-/-}$ macrophages, mice were weaned onto normal chow and used at 8–12 wk of age. For experiments involving *Apoe*$^{-/-}$ and *Atf3*$^{-/-}$*Apoe*$^{-/-}$ macrophages or mice, mice were weaned onto a high-fat diet (protein, 17.3% wt/wt; carbohydrate, 48.5% wt/wt; fat, 21.2% wt/wt; cholesterol, 0.2% wt/wt; Teklad; Harlan) for 8 wk. All experimental animals used for atherosclerosis studies were bread and maintained at the animal facility of the Institute for Systems Biology. All animals were housed and handled in accordance with a protocol approved by the Institute for Systems Biology's Institutional Animal Care and Use Committee. Mice were sacrificed by CO_2 asphyxiation and tissues/cells were obtained as described in the next section. Whole blood was extracted postmortem by cardiac puncture and serum was obtained using a serum separator vacutainer (BD). Serum samples were assayed for TG and total cholesterol using fast protein liquid chromatography.

Cell culture
Cells were cultured at 37°C and in 5% CO_2 in a humidified incubator. Primary mouse BMDMs were prepared as previously described (Gilchrist et al., 2006). In brief, femoral BM cells were plated on non–tissue culture–treated plastic in BMDM medium (RPMI 1640 containing L-glutamine [Invitrogen], supplemented with 10% [vol/vol] FBS [Invitrogen] that had been heat-inactivated [30 min at 56°C], 100 IU/ml penicillin [Cellgro], 100 µg/ml streptomycin [Cellgro], and 50 ng/ml rhM-CSF [Chiron]). On day 4, the medium was replaced, and on day 6, adherent cells were lifted in PBS + 1 mM EDTA, counted, pelleted, resuspended in BMDM medium, and plated as described in the next section. On day 7, cells were stimulated as indicated in the Results section, before being used for microscopy, flow cytometry, RNA extraction, or lipid extraction. Stimuli that were introduced into BMDM medium (as indicated in the text) were as follows: LPS (from *Salmonella minnesota*; List Biological Laboratories), nLDL (Intracel), acLDL (Intracel), CuSO₄-oxLDL (Intracel), cholesterol (Sigma-Aldrich), or 25-HC (Avanti Polar Lipids). Intracel-sourced lipoproteins were derived from fresh human plasma containing EDTA, filtered at 0.45 µm, and quantitated for protein content using a BCA assay (Thermo Fisher Scientific). Peritoneal macrophages were isolated as follows. Peritoneal exudate cells (PECs) were obtained by i.p. lavage with 8 ml of ice-cold PBS. PECs were counted, pelleted, resuspended in complete RPMI (at 4× the cell densities used for resuspending day 6 BMDM), and plated onto coverslips or into tissue culture dishes as described in the next section. Cells were incubated for 2 h and then nonadherent cells were removed by washing 3× with PBS. FBS-supplemented medium and oxLDL were assayed for endotoxin using a limulus amebocyte lysate gel-clot reagent (Charles River) with a limit of detection of 0.030 EU/ml. Based on this assay, FBS-supplemented medium contained between 0.12 and 0.30 EU/ml. oxLDL contained between 0.1 and 0.75 EU/ml, comparable to the FBS-containing medium. These values are two to three orders of magnitude below the LPS concentrations used to TLR4-activate macrophages (100–200 EU/ml). Heat-inactivated FBS was also assayed for the levels of free and total cholesterol using the Amplex Red Cholesterol Assay kit (Invitrogen). From these measurements, the FBS levels of free cholesterol and CE were determined to be 7.9 and 42.5 mg/dl, respectively. In a BMDM suspension at standard cell density in BMDM medium supplemented with 10% FBS, cells are therefore supplemented with CE at ∼60 pg/cell.

Microscopy
50 µl of cell suspension (containing 50,000 BMDM or 200,000 PECs) in medium was dispensed onto a #1.5 coverslip in a 24-well plate. Cells were allowed to adhere for 2 h. (For PECs, coverslips were then washed as described in the previous section). The volume of medium was brought up to 250 µl/well. After cells were incubated with appropriate stimulation as described in the text, medium was removed. For single-color (BODIPY or Nile red) microscopy, coverslips were prepared as follows: fixed in 10% formalin for 15 min; incubated in PBS with 10 µM BODIPY 493/503 (Invitrogen) for 30 min in the dark or with 1 µg/ml Nile red (Sigma-Aldrich) for 5 min at RT in the dark; and washed 3× with PBS. For two-color fluorescence microscopy (ADRP + BODIPY), coverslips were prepared as follows: washed 2× with PBS; fixed in 3% paraformaldehyde for 20 min and washed 3× with PBS; permeabilized by incubation in reagent diluent (PBS with 0.1 mg/ml saponin and 0.5 mg/ml BSA) with 0.2 M glycine for 45 min; incubated with 1:50 dilution of α–ADRP polyclonal antibody (Fitzgerald) in reagent diluent for 1 h; washed 3× with PBS; incubated in reagent diluent with 1:250 dilution of labeled secondary (anti–guinea pig Alexa Fluor 633 conjugate) and 10 µM BODIPY for 1 h in the dark; and washed 4× with PBS. Coverslips were mounted to microscope slides using Vectashield hard-set mounting medium (Vector Laboratories). Confocal micrographs were acquired using a laser scanning confocal microscope (TCS SP2; Leica), in 512 × 512 scan mode, at room temperature, using a 100× oil-immersion objective (1.4 NA; Leica). Confocal images in

Fig. 1 (A–D) were acquired at 3× zoom. Confocal images in Figs. 2 and 3 were acquired at 1× zoom. Fluorophores were excited using a 488–nm laser line (for BODIPY and Nile red) and a 633–nm laser line (for Alexa Fluor 633), and emission filters were configured using the default instrument settings for FITC (for BODIPY and Nile red) and Cy5 (for Alexa Fluor 633). Image acquisition was performed using the LCS software (Leica). Addition of scale bars and merging of color channels was performed using ImageJ software (National Institutes of Health).

Lipid body quantitation
BMDMs were plated on coverslips as described in Cell culture, and incubated for 18 h in media containing modified lipoproteins, LPS, or media alone, as described in the Results. Cells were fixed and stained with BODIPY as described in Cell culture. For each coverslip, five fields were imaged using the confocal microscope as described in Cell culture (with 1× zoom, ∼7.5 cells/field), except that BODIPY fluorescence and bright-field images were obtained in stacks of 20 Z-positions over the range of positions at which the cells were in focus (5–12 µm). Cells were segmented using the variance of the bright-field image through the Z-stack, as described previously (Selinummi et al., 2009). Cellular lipid bodies were detected from the stacked fluorescence images, eliminating lipid bodies which are redundant in the stack, using a custom algorithm implemented in the CellProfiler software (Carpenter et al., 2006), as described previously (Ruusuvuori et al., 2010). The total pixel area of lipid bodies within a field was computed, and then divided by the number of cells to obtain the mean lipid body pixel area per cell.

Flow cytometry
500 µl of a suspension of macrophages (3×10^5 BMDM or 1.2×10^6 PECs) in medium was plated per well into a 12-well, non–TC–treated tissue culture plate. For PECs, cells were allowed to adhere for 2 h and were washed as described in Cell culture. Cells were stimulated as described in the Results section. Medium was removed and cells were lifted by incubation in PBS + 1 mM EDTA. Cells were pelleted, resuspended in 50 µl of 10% formalin, incubated for 15 min at 4°C, pelleted, resuspended in FACS buffer (PBS with 2% FBS and 2 mM EDTA) containing 10 µM BODIPY, and incubated for 30 min in the dark. Cells were washed in FACS buffer, pelleted, and resuspended in FACS buffer (PBS with 2% FBS and 2 mM EDTA) with 2.5% formalin. Up to 50,000 events were detected using the FACSCalibur (BD) with excitation using the 488-nm laser and acquisition enabled for forward light scatter, side scatter, and fluorescence emission (530/30 nm filter). The CellQuest Pro software was used for data acquisition. Data analysis was performed using FlowJo software (version 8.8.7; Tree Star). Events were gated on forward and side scatter to select the main population of cells, and the counts distribution for the 530/30 fluorescence emission channel was generated for the gated events.

25–HC analysis
For analysis of 25-HC in aortas, whole aortas were dissected immediately postmortem and homogenized in 1 ml PBS in a TissueLyser II (QIAGEN) for 6 min at a frequency of 30 Hz. The homogenate was transferred to a new tube, the homogenization tube was washed with 600 µl PBS, and the combined volume was used as the starting point for lipid extraction. For cells and cell-conditioned media, on day 6, 22.5 ml of BMDM medium containing a suspension of 16 million BMDM was plated into a 15-cm Petri dish. For analysis of 25-HC in cells, on day 7, cells were lifted, pelleted, and resuspended in 1.6 ml PBS before addition of chloroform/methanol. For analysis of 25-HC in cell-conditioned media, nLDL was added on day 6, cells were incubated for 24 h, and 1.6 ml of medium was sampled for lipid extraction. For each sample type (aorta, cells, or medium), 1.6 ml of aqueous sample was added to 6 ml 1:2 (vol/vol) chloroform/methanol spiked with 500 pmol d3 25-HC (Avanti Polar Lipids, Inc.) and (in the case of aortas) 5 nmol of day 7 cholesterol (Avanti Polar Lipids, Inc.). Bulk lipid extraction and sterol isolation were performed according to a published protocol (McDonald et al., 2007). Sterol samples were evaporated under N_2 gas using the N-EVAP apparatus (Organomation), dissolved in 50 µl of ethanol, and then fractionated

using reverse-phase HPLC on an Agilent 1100 system according to a published protocol (Rodriguez, 2004), which was modified as follows: an XTerra RP-18 column (2.1 × 150 mm, 3.5 µm particle size; Waters) was used, with an injection volume of 50 µl and a flow rate of 0.25 ml/min. Acetonitrile (ACN) was used as the organic solvent and the aqueous buffer was H_2O containing 1 mM H_3PO_4. The gradient schedule was as follows: 0–5 min, 65% ACN; 5–25 min, ramp from 65% to 100% ACN; 25–35 min, 100% ACN; 35–45 min, 65% ACN. The retention times of 25-HC and cholesterol were determined to be ∼11 and 25 min, respectively. For each analyte (25-HC and cholesterol), two fractions were collected in two 2-min bins (each) bracketing the analyte's retention time. The SpeedVac-evaporated sterol fractions were redissolved in chloroform/methanol and infused at 2 µl/min into a QSTAR (Applied Biosystems) or a QTOF (Waters) configured for electrospray ionization mass spectrometry (ESI-MS) in positive ion mode. Unmodified 25-HC was detected with (parent, fragment) ion m/z values (420.4, 367.4); cholesterol was detected at m/z values (404.4, 369.4). For each analyte, a five-point calibration curve was obtained from a serial dilution of standard, with a linear fit to the calibration data on log-log scale. To correct for differences in extraction efficiency between analytes, the abundance level for each analyte was normalized to the abundance level for the isotope-labeled standard within each biological sample.

Lipidomic analysis of CE and TG
BMDM of the indicated genotypes were incubated for 7 d and lifted as described in Cell culture. Cells were pelleted and resuspended in PBS, and then lysed using ceramic bead disruption. Cell lysate was assayed for total protein content using the BCA method (Thermo Fisher Scientific). A volume containing 600 pmol of 19:0 cholesterol ester (Lipid MAPS ID LMST01020002; Avanti Polar Lipids, Inc.) and 30 pmol of each of eight day-5–labeled TAG internal standards (LM-6000; Avanti Polar Lipids, Inc.) was added to a volume of lysate corresponding to a fixed amount of total protein (123 µg). Total lipid was extracted using a modified Folch method (Folch et al., 1957). Neutral lipids were obtained from the total lipid extract by solid-phase extraction according to a previously published method (Krank et al., 2007). In brief, the total lipid extract was evaporated under N_2 gas, redissolved in 1 ml iso-octane/ethyl acetate (75:25 vol/vol), sonicated, and then loaded onto silica cartridges (Isolute silica cartridges, size XL; Biotage). Neutral lipids were eluted with isooctane/ethyl acetate (75:25 vol/vol), evaporated under N_2 gas, and dissolved in 1 ml chloroform/methanol (1:2 vol/vol) containing 7.5 mM ammonium acetate. Neutral lipid samples were assayed for CE and TG species using ESI-MS in precursor-ion and neutral-loss scanning modes on a 4000 QTRAP (Applied Biosystems) hybrid quadrupole/linear ion trap mass spectrometer (Applied Biosystems), at an infusion rate of 5 µl/min with a 40-min run time. Data were analyzed for total CE and TG signal using LipidView software version 1.1 (AB Sciex).

Histopathology
Aortas were flushed with PBS, fixed in 10% formalin, embedded in paraffin, and the aortic root was sectioned at 4 µm thickness. Every 10th section was stained with Movat's pentachrome for lesion area quantitation. Additionally, for each animal, three serial sections were stained for Mac-2 (macrophage marker), SM α actin (smooth muscle cell marker), and CD3 (T cell marker), respectively. Immunostained sections were then stained with HRP-conjugated secondary and counterstained with hematoxylin. Images were acquired on a microscope (BX 50; Olympus) with a 10× Plan objective (Olympus) and a camera (EOS 5D Mark II; Canon). Quantitation was performed in Image Pro Plus software (6.0; Media Cybernetics). Scale bars were added using ImageJ. Lesion area was determined as a mean of the five sections per aortic root. For visualizing neutral lipids in tissue sections, formalin-fixed, 10% sucrose-infused, OCT-embedded frozen sections were stained with Oil red O and counterstained with hematoxylin. Images were obtained as described for the immunostained tissue sections.

Microarray analysis
Affymetrix exon array. Day 6 BMDMs from female mice of the indicated genotypes were plated at 10^6 cells/well into 6-well tissue culture-treated

plates, in BMDM medium. On day 7, cells were stimulated as indicated, and total RNA was isolated using TRIzol (Invitrogen). RNA quality was analyzed with a 2100 Bioanalyzer (Agilent Technologies). Sample mRNA was amplified and labeled with One-Cycle Eukaryotic Target Labeling Assay protocol and reagents (Affymetrix). Labeled cDNA was hybridized to a GeneChip Mouse Exon 1.0 ST array (as indicated in the Results section; Affymetrix) using standard protocols and reagents (Affymetrix). Imaging was performed with the GeneChip Scanner 3000 (Affymetrix) and the images were processed into probe-level intensities using GeneChip Operating Software (Affymetrix). Probe intensities were quantile-normalized and probe set–summarized (separately using exon-level and transcript-level probe sets) using the PLIER algorithm (Affymetrix) as implemented in the Power Tools software suite (Affymetrix). The probe set summarization was performed using probe–to–probe set mappings from the CustomCDF Project based on the Ensembl Exon and Ensembl Transcript databases (CustomCDF Version 13). Exon-level present/absent calls were made using the detection above background (DABG; Affymetrix) algorithm with a p-value cutoff of 0.01. Transcript present/absent calls were made by requiring that at least 50% of the exons for that transcript have a present call (See the Affymetrix technical note Identifying and validating alternative splicing events: an introduction to managing data provided by GeneChip® exon arrays; http://media.affymetrix.com/support/technical/technotes/id_altsplicingevents_technote.pdf). For the heat map in Fig. 2 F, for each gene, a representative transcript was selected that had the highest mean $\log_2$ transcript-level probe set intensity within any of the four conditions. All microarray datasets are available through National Center for Biotechnology Information GEO, as indicated in Table 1. Accession nos. for the datasets are GSE32358, GSE32359, and GSE32574.

Affymetrix 3′ array. The 3′ microarray data files used to generate Fig. 3 B were a subset of the microarray data files used in (Gilchrist et al., 2006) corresponding to WT and $Atf3^{-/-}$ unstimulated and 4-h LPS-stimulated BMDM. The probe-level data files were reanalyzed using up-to-date genome annotations. Probe intensities were background-adjusted, quantile-normalized, and probe set–summarized according to the Robust Multichip Average procedure (Irizarry et al., 2003), using the affy package (version 1.22.1) in the Bioconductor software package, and using the Ensembl Gene–based probe set mapping file (version 13, based on Ensembl Mm_60) from the CustomCDF project (Dai et al., 2005).

Immunoprecipitation and ChIP–seq

BMDMs were cultured from female mice of the indicated genotypes and, on day 7, cells were stimulated with oxLDL as described in the Results section. Immunoprecipitation (IP) was performed as described in Gilchrist et al. (2006), except that Protein A Dynabeads (Invitrogen) were used in place of agarose beads. Antibodies used for IP were as follows: acetyl-H4 IP (rabbit polyclonal IgG; Millipore); and ATF3 (rabbit polyclonal IgG; Santa Cruz Biotechnology, Inc.). For ChIP-qPCR at the *Ch25h* promoter, the primers used were as follows: forward primer, 5′-TAGCAGCCCATGCTGAGACTATGT-3′; reverse primer, 5′-TTCTTTAGCAGGGAAAGGGAGGTG-3′; and probe, 56-FAM/AGTGACGTCACCCTTCCGTCTCCTT/36-TAMSp (IDT). From the acetyl-H4 IP, a sequencing library was derived using the Illumina reagent kit, and 36-cycle, single-ended sequencing was performed on a Genome Analyzer II (Illumina). ChIP-seq data processing, mapping of reads to the mouse genome assembly (NCBI37), and peak detection were performed as described previously (Ramsey et al., 2010b).

Combined analysis of transcriptional and ChIP–seq data

Among Ensembl transcripts called as present in WT BMDM, differential expression testing was performed between the sample groups LPS versus no stimulation and between the sample groups oxLDL versus no stimulation. Any transcript for which the p-value for differential expression (see Statistical analysis) was >0.01 was excluded from further analysis. For the combined analysis with ChIP-seq data, any transcript for which the fold change was <8 (for LPS) or <2 (for oxLDL) was excluded from further analysis. An additional set of 500 background transcripts was randomly selected from a list of transcripts

that are expressed in BMDM in any of the following three conditions: unstimulated, LPS treated, or oxLDL treated. Promoter regions within ±1 kbp of the transcription start site of these LPS– or oxLDL–up-regulated transcripts, along with the background transcripts, were obtained from Ensembl (Mm_60). All histone-acetylated (HAc) locations within these promoter regions were identified by taking the base pair–level intersection of the promoter regions with the set of all regions identified as histone-acetylated in WT macrophages in any of the conditions (unstimulated, 4-h LPS-treated, or 24-h oxLDL-treated), using the University of California, Santa Cruz (UCSC) genome browser (NCBI37 assembly). These regions were extended symmetrically so that each region was at least 400 bp. Using the UCSC genome browser, the resulting three sets of mouse genomic regions (HAc regions within the promoters of background genes, HAc regions within the promoters of LPS–up-regulated genes, and HAc regions within the promoters of oxLDL–up-regulated genes) were mapped to sequence files for TF binding site motif analysis.

TF binding site motif analysis

Sequence files were scanned using the position-weight matrix scanning program Clover (Frith et al., 2004), and using all vertebrate TF binding site matrices from the TRANSFAC Professional 2010 database (BioBase). Separate statistical tests were performed to identify TF binding site motifs that were statistically overrepresented (P < 0.001, based on the empirical p-value estimate from the Clover program) within the LPS-derived sequences (vs. within background sequences) and within the oxLDL-derived sequences (vs. background). TF binding site motifs that were overrepresented within both the LPS- and oxLDL-derived sequences were tabulated, corresponding to 10 unique motifs (Fig. 1 F).

cDNA and qPCR

Total RNA was isolated with TRIzol reagent (Invitrogen), DNase-treated using the Turbo DNase kit (Ambion), reverse transcribed using SuperScript II (Invitrogen), and analyzed by real-time PCR with TaqMan Gene Expression assays (Applied Biosystems) in a 10-µl reaction volume, on a 7900 Fast Real-Time PCR system (Applied Biosystems). TaqMan assays that were used are: *Atf3* (Mm00476032_m1), *Ch25h* (Mm00515486_s1), and *Gapdh* (Mm99999915_g1). For *Eef1a1*, the primers used were as follows: forward primer, 5′-GCAAAAACGACCCACCAATG-3′; reverse primer, 5′-GGCTGGATGGTTCAGGATA-3′; and probe, 56-FAM/CACCTGAGCAGTGAAGCCAG/36-TAMSp (IDT). Data were normalized to the expression levels of *Eef1a1* or *Gapdh* mRNA (as indicated in the text) within individual samples.

Statistical analysis

Differential expression testing for microarray responses of WT BMDM to LPS or to oxLDL was performed using a two-tailed Student's *t* test on the $\log_2$ probe set intensities for hybridizations from each sample group, using Excel (Microsoft). Differential expression testing for effect of ATF3 KO on responses of BMDM in the presence or absence of oxLDL was performed on the $\log_2$ intensities using a two-way ANOVA test in R, and the p-value cutoff at an estimated gene-level false discovery rate of 0.1 (P < 2.26 × 10⁻³) was determined using the Benjamini-Hochberg procedure (Benjamini and Hochberg, 1995). Aortic root lesion areas were analyzed using a two-way ANOVA test with sex and genotype as factors, using Prism 5 software (GraphPad Software).

Online supplemental material

Lists of transcripts that are differentially expressed (at least twofold) under LPS stimulation or under oxLDL stimulation in WT BMDM are provided as Tables S1 (LPS) and S2 (oxLDL). ChIP-seq peak locations for acetyl-H4 (in unstimulated, LPS-stimulated, or oxLDL-stimulated BMDM) are provided in a UCSC BED format file as Table S3. A list of transcripts that are differentially expressed (at least twofold) in $Atf3^{-/-}$ versus WT BMDM (FDR < 0.1) is provided in Table S4. Online supplemental material is available at http://www.jem.org/cgi/content/full/jem.20111202/DC1.

REFERENCES

Bauman, D.R., A.D. Bitmansour, J.G. McDonald, B.M. Thompson, G. Liang, and D.W. Russell. 2009. 25-Hydroxycholesterol secreted by macrophages in response to Toll-like receptor activation suppresses immunoglobulin A production. *Proc. Natl. Acad. Sci. USA.* 106:16764–16769. http://dx.doi.org/10.1073/pnas.0909142106

Benjamini, Y., and Y. Hochberg. 1995. Controlling the false discovery rate: a practical and powerful approach to multiple testing. *J.R. Stat. Soc. Ser. B.* 57:289–300.

Bozza, P.T., R.C. Melo, and C. Bandeira-Melo. 2007. Leukocyte lipid bodies regulation and function: contribution to allergy and host defense. *Pharmacol. Ther.* 113:30–49. http://dx.doi.org/10.1016/j.pharmthera.2006.06.006

Brown, M.S., S.E. Dana, and J.L. Goldstein. 1975. Cholesterol ester formation in cultured human fibroblasts. Stimulation by oxygenated sterols. *J. Biol. Chem.* 250:4025–4027.

Caligiuri, G., A. Nicoletti, X. Zhou, I. Törnberg, and G.K. Hansson. 1999. Effects of sex and age on atherosclerosis and autoimmunity in apoE-deficient mice. *Atherosclerosis.* 145:301–308. http://dx.doi.org/10.1016/S0021-9150(99)00081-7

Carpenter, A.E., T.R. Jones, M.R. Lamprecht, C. Clarke, I.H. Kang, O. Friman, D.A. Guertin, J.H. Chang, R.A. Lindquist, J. Moffat, et al. 2006. CellProfiler: image analysis software for identifying and quantifying cell phenotypes. *Genome Biol.* 7:R100. http://dx.doi.org/10.1186/gb-2006-7-10-r100

Castrillo, A., and P. Tontonoz. 2004. Nuclear receptors in macrophage biology: at the crossroads of lipid metabolism and inflammation. *Annu. Rev. Cell Dev. Biol.* 20:455–480. http://dx.doi.org/10.1146/annurev.cellbio.20.012103.134432

Chen, S.C., Y.C. Liu, K.G. Shyu, and D.L. Wang. 2008. Acute hypoxia to endothelial cells induces activating transcription factor 3 (ATF3) expression that is mediated via nitric oxide. *Atherosclerosis.* 201:281–288. http://dx.doi.org/10.1016/j.atherosclerosis.2008.02.014

Dai, M., P. Wang, A.D. Boyd, G. Kostov, B. Athey, E.G. Jones, W.E. Bunney, R.M. Myers, T.P. Speed, H. Akil, et al. 2005. Evolving gene/transcript definitions significantly alter the interpretation of GeneChip data. *Nucleic Acids Res.* 33:e175. http://dx.doi.org/10.1093/nar/gni179

Diczfalusy, U., K.E. Olofsson, A.M. Carlsson, M. Gong, D.T. Golenbock, O. Rooyackers, U. Fläring, and H. Björkbacka. 2009. Marked upregulation of cholesterol 25-hydroxylase expression by lipopolysaccharide. *J. Lipid Res.* 50:2258–2264. http://dx.doi.org/10.1194/jlr.M900107-JLR200

Du, X., Y.H. Pham, and A.J. Brown. 2004. Effects of 25-hydroxycholesterol on cholesterol esterification and sterol regulatory element-binding protein processing are dissociable: implications for cholesterol movement to the regulatory pool in the endoplasmic reticulum. *J. Biol. Chem.* 279:47010–47016. http://dx.doi.org/10.1074/jbc.M408690200

Ecker, J., G. Liebisch, M. Englmaier, M. Grandl, H. Robenek, and G. Schmitz. 2010. Induction of fatty acid synthesis is a key requirement for phagocytic differentiation of human monocytes. *Proc. Natl. Acad. Sci. USA.* 107:7817–7822. http://dx.doi.org/10.1073/pnas.0912059107

Field, F.J., E. Born, S. Murthy, and S.N. Mathur. 2001. Regulation of sterol regulatory element-binding proteins by cholesterol flux in CaCo-2 cells. *J. Lipid Res.* 42:1687–1698.

Folch, J., M. Lees, and G.H. Sloane Stanley. 1957. A simple method for the isolation and purification of total lipides from animal tissues. *J. Biol. Chem.* 226:497–509.

Frith, M.C., Y. Fu, L. Yu, J.F. Chen, U. Hansen, and Z. Weng. 2004. Detection of functional DNA motifs via statistical over-representation. *Nucleic Acids Res.* 32:1372–1381. http://dx.doi.org/10.1093/nar/gkh299

Fujimoto, Y., H. Itabe, J. Sakai, M. Makita, J. Noda, M. Mori, Y. Higashi, S. Kojima, and T. Takano. 2004. Identification of major proteins in the lipid droplet-enriched fraction isolated from the human hepatocyte cell line HuH7. *Biochim. Biophys. Acta.* 1644:47–59. http://dx.doi.org/10.1016/j.bbamcr.2003.10.018

Gilchrist, M., V. Thorsson, B. Li, A.G. Rust, M. Korb, J.C. Roach, K. Kennedy, T. Hai, H. Bolouri, and A. Aderem. 2006. Systems biology approaches identify ATF3 as a negative regulator of Toll-like receptor 4. *Nature.* 441:173–178. http://dx.doi.org/10.1038/nature04768

Greaves, D.R., and S. Gordon. 2005. Thematic review series: the immune system and atherogenesis. Recent insights into the biology of macrophage scavenger receptors. *J. Lipid Res.* 46:11–20. http://dx.doi.org/10.1194/jlr.R400011-JLR200

Greaves, D.R., and S. Gordon. 2009. The macrophage scavenger receptor at 30 years of age: current knowledge and future challenges. *J. Lipid Res.* 50:S282–S286. http://dx.doi.org/10.1194/jlr.R800066-JLR200

Hai, T., C.D. Wolfgang, D.K. Marsee, A.E. Allen, and U. Sivaprasad. 1999. ATF3 and stress responses. *Gene Expr.* 7:321–335.

Hartman, M.G., D. Lu, M.L. Kim, G.J. Kociba, T. Shukri, J. Buteau, X. Wang, W.L. Frankel, D. Guttridge, M. Prentki, et al. 2004. Role for activating transcription factor 3 in stress-induced beta-cell apoptosis. *Mol. Cell. Biol.* 24:5721–5732. http://dx.doi.org/10.1128/MCB.24.13.5721-5732.2004

Imanishi, Y., V. Gerke, and K. Palczewski. 2004. Retinosomes: new insights into intracellular managing of hydrophobic substances in lipid bodies. *J. Cell Biol.* 166:447–453. http://dx.doi.org/10.1083/jcb.200405110

Irizarry, R.A., B.M. Bolstad, F. Collin, L.M. Cope, B. Hobbs, and T.P. Speed. 2003. Summaries of Affymetrix GeneChip probe level data. *Nucleic Acids Res.* 31:e15. http://dx.doi.org/10.1093/nar/gng015

Johnson, K.A., C.J. Morrow, G.D. Knight, and T.J. Scallen. 1994. *In vivo* formation of 25-hydroxycholesterol from endogenous cholesterol after a single meal, dietary cholesterol challenge. *J. Lipid Res.* 35:2241–2253.

Kandutsch, A.A., and H.W. Chen. 1975. Regulation of sterol synthesis in cultured cells by oxygenated derivatives of cholesterol. *J. Cell. Physiol.* 85:415–424. http://dx.doi.org/10.1002/jcp.1040850408

Kim, E.Y., H.Y. Shin, J.Y. Kim, D.G. Kim, Y.M. Choi, H.K. Kwon, D.K. Rhee, Y.S. Kim, and S. Choi. 2010. ATF3 plays a key role in Kdo2-lipid A-induced TLR4-dependent gene expression via NF-κB activation. *PLoS ONE.* 5:e14181. http://dx.doi.org/10.1371/journal.pone.0014181

Krank, J., R.C. Murphy, R.M. Barkley, E. Duchoslav, and A. McAnoy. 2007. Qualitative analysis and quantitative assessment of changes in neutral glycerol lipid molecular species within cells. *Methods Enzymol.* 432:1–20. http://dx.doi.org/10.1016/S0076-6879(07)32001-6

Li-Hawkins, J., E.G. Lund, S.D. Turley, and D.W. Russell. 2000. Disruption of the oxysterol 7α-hydroxylase gene in mice. *J. Biol. Chem.* 275:16536–16542. http://dx.doi.org/10.1074/jbc.M001811200

Litvak, V., S.A. Ramsey, A.G. Rust, D.E. Zak, K.A. Kennedy, A.E. Lampano, M. Nykter, I. Shmulevich, and A. Aderem. 2009. Function of C/EBPdelta in a regulatory circuit that discriminates between transient and persistent TLR4-induced signals. *Nat. Immunol.* 10:437–443. http://dx.doi.org/10.1038/ni.1721

Lundberg, B. 1985. Chemical composition and physical state of lipid deposits in atherosclerosis. *Atherosclerosis.* 56:93–110. http://dx.doi.org/10.1016/0021-9150(85)90087-5

Maxfield, F.R., and I. Tabas. 2005. Role of cholesterol and lipid organization in disease. *Nature.* 438:612–621. http://dx.doi.org/10.1038/nature04399

McDonald, J.G., B.M. Thompson, E.C. McCrum, and D.W. Russell. 2007. Extraction and analysis of sterols in biological matrices by high performance liquid chromatography electrospray ionization mass spectrometry. *Methods Enzymol.* 432:145–170. http://dx.doi.org/10.1016/S0076-6879(07)32006-5

Melo, R.C., H. D'Avila, H.C. Wan, P.T. Bozza, A.M. Dvorak, and P.F. Weller. 2011. Lipid bodies in inflammatory cells: structure, function, and current imaging techniques. *J. Histochem. Cytochem.* 59:540–556. http://dx.doi.org/10.1369/0022155411404073

Miller, S.C., and G. Melnykovych. 1984. Regulation of cholesterol biosynthesis and esterification by 25-hydroxycholesterol in a macrophage-like cell line: uncoupling by progesterone. *J. Lipid Res.* 25:991–999.

Moore, K.J., and I. Tabas. 2011. Macrophages in the pathogenesis of atherosclerosis. *Cell.* 145:341–355. http://dx.doi.org/10.1016/j.cell.2011.04.005

Nakashima, Y., A.S. Plump, E.W. Raines, J.L. Breslow, and R. Ross. 1994. ApoE-deficient mice develop lesions of all phases of atherosclerosis throughout the arterial tree. *Arterioscler. Thromb.* 14:133–140. http://dx.doi.org/10.1161/01.ATV.14.1.133

Nawa, T., M.T. Nawa, M.T. Adachi, I. Uchimura, R. Shimokawa, K. Fujisawa, A. Tanaka, F. Numano, and S. Kitajima. 2002. Expression of transcriptional repressor ATF3/LRF1 in human atherosclerosis: co-localization and possible involvement in cell death of vascular endothelial cells. *Atherosclerosis.* 161:281–291. http://dx.doi.org/10.1016/S0021-9150(01)00639-6

Nicolaou, G., and C. Erridge. 2010. Toll-like receptor-dependent lipid body formation in macrophage foam cell formation. *Curr. Opin. Lipidol.* 21:427–433. http://dx.doi.org/10.1097/MOL.0b013e32833cacd5

Okamoto, A., Y. Iwamoto, and Y. Maru. 2006. Oxidative stress-responsive transcription factor ATF3 potentially mediates diabetic angiopathy. *Mol. Cell. Biol.* 26:1087–1097. http://dx.doi.org/10.1128/MCB.26.3.1087-1097.2006

Park, K., and A.L. Scott. 2010. Cholesterol 25-hydroxylase production by dendritic cells and macrophages is regulated by type I interferons. *J. Leukoc. Biol.* 88:1081–1087. http://dx.doi.org/10.1189/jlb.0610318

Pereira, J.P., L.M. Kelly, and J.G. Cyster. 2010. Finding the right niche: B-cell migration in the early phases of T-dependent antibody responses. *Int. Immunol.* 22:413–419. http://dx.doi.org/10.1093/intimm/dxq047

Ramsey, S.A., S.L. Klemm, D.E. Zak, K.A. Kennedy, V. Thorsson, B. Li, M. Gilchrist, E.S. Gold, C.D. Johnson, V. Litvak, et al. 2008. Uncovering a macrophage transcriptional program by integrating evidence from motif scanning and expression dynamics. *PLOS Comput. Biol.* 4:e1000021. http://dx.doi.org/10.1371/journal.pcbi.1000021

Ramsey, S.A., E.S. Gold, and A. Aderem. 2010a. A systems biology approach to understanding atherosclerosis. *EMBO Mol Med.* 2:79–89. http://dx.doi.org/10.1002/emmm.201000063

Ramsey, S.A., T.A. Knijnenburg, K.A. Kennedy, D.E. Zak, M. Gilchrist, E.S. Gold, C.D. Johnson, A.E. Lampano, V. Litvak, G. Navarro, et al. 2010b. Genome-wide histone acetylation data improve prediction of mammalian transcription factor binding sites. *Bioinformatics.* 26:2071–2075. http://dx.doi.org/10.1093/bioinformatics/btq405

Rodriguez, I.R. 2004. Rapid analysis of oxysterols by HPLC and UV spectroscopy. *Biotechniques.* 36:952–954: 956: 958.

Ruusuvuori, P., T. Aijö, S. Chowdhury, C. Garmendia-Torres, J. Selinummi, M. Birbaumer, A.M. Dudley, L. Pelkmans, and O. Yli-Harja. 2010. Evaluation of methods for detection of fluorescence labeled subcellular objects in microscope images. *BMC Bioinformatics.* 11:248. http://dx.doi.org/10.1186/1471-2105-11-248

Seimon, T.A., M.J. Kim, A. Blumenthal, J. Koo, S. Ehrt, H. Wainwright, L.G. Bekker, G. Kaplan, C. Nathan, I. Tabas, and D.G. Russell. 2010. Induction of ER stress in macrophages of tuberculosis granulomas. *PLoS ONE.* 5:e12772. http://dx.doi.org/10.1371/journal.pone.0012772

Selinummi, J., P. Ruusuvuori, I. Podolsky, A. Ozinsky, E. Gold, O. Yli-Harja, A. Aderem, and I. Shmulevich. 2009. Bright field microscopy as an alternative to whole cell fluorescence in automated analysis of macrophage images. *PLoS ONE.* 4:e7497. http://dx.doi.org/10.1371/journal.pone.0007497

Shibata, N., and C.K. Glass. 2010. Macrophages, oxysterols and atherosclerosis. *Circ. J.* 74:2045–2051. http://dx.doi.org/10.1253/circj.CJ-10-0860

Silva, A.R., P. Pacheco, A. Vieira-de-Abreu, C.M. Maya-Monteiro, B. D'Alegria, K.G. Magalhães, E.F. de Assis, C. Bandeira-Melo, H.C. Castro-Faria-Neto, and P.T. Bozza. 2009. Lipid bodies in oxidized LDL-induced foam cells are leukotriene-synthesizing organelles: a MCP-1/CCL2 regulated phenomenon. *Biochim. Biophys. Acta.* 1791:1066–1075.

Smith, J.D., and J.L. Breslow. 1997. The emergence of mouse models of atherosclerosis and their relevance to clinical research. *J. Intern. Med.* 242:99–109. http://dx.doi.org/10.1046/j.1365-2796.1997.00197.x

Taylor, F.R. 1992. Correlation among oxysterol potencies in the regulation of the degradation of 3-hydroxy-3-methylglutaryl CoA reductase, the repression of 3-hydroxy-3-methylglutaryl CoA synthase and affinities for the oxysterol receptor. *Biochem. Biophys. Res. Commun.* 186:182–189. http://dx.doi.org/10.1016/S0006-291X(05)80791-0

Trzaskos, J.M., M. Jonas, and H.W. Chen. 1989. Sterol-mediated suppression of HMG-CoA reductase mRNA levels in cultured cells requires protein synthesis. *Biochem. Biophys. Res. Commun.* 161:267–271. http://dx.doi.org/10.1016/0006-291X(89)91590-8

Vettese-Dadey, M., P.A. Grant, T.R. Hebbes, C. Crane-Robinson, C.D. Allis, and J.L. Workman. 1996. Acetylation of histone H4 plays a primary role in enhancing transcription factor binding to nucleosomal DNA *in vitro. EMBO J.* 15:2508–2518.

Zak, D.E., and A. Aderem. 2009. Systems biology of innate immunity. *Immunol. Rev.* 227:264–282. http://dx.doi.org/10.1111/j.1600-065X.2008.00721.x

Zak, D.E., F. Schmitz, E.S. Gold, A.H. Diercks, J.J. Peschon, J.S. Valvo, A. Niemistö, I. Podolsky, S.G. Fallen, R. Suen, et al. 2011. Systems analysis identifies an essential role for SHANK-associated RH domain-interacting protein (SHARPIN) in macrophage Toll-like receptor 2 (TLR2) responses. *Proc. Natl. Acad. Sci. USA.* 108:11536–11541. http://dx.doi.org/10.1073/pnas.1107577108

Zhao, B., B.J. Fisher, R.W. St Clair, L.L. Rudel, and S. Ghosh. 2005. Redistribution of macrophage cholesteryl ester hydrolase from cytoplasm to lipid droplets upon lipid loading. *J. Lipid Res.* 46:2114–2121. http://dx.doi.org/10.1194/jlr.M500207-JLR200

Zmuda, E.J., L. Qi, M.X. Zhu, R.G. Mirmira, M.R. Montminy, and T. Hai. 2010. The roles of ATF3, an adaptive-response gene, in high-fat-diet–induced diabetes and pancreatic beta-cell dysfunction. *Mol. Endocrinol.* 24:1423–1433. http://dx.doi.org/10.1210/me.2009-0463